Chapter 4

Impact of 13-93 bioactive glass addition on the structural, mechanical, *in-vitro* degradation, cell culture, and antibacterial response of the 3Y-TZP-based biocomposite materials

4.1 Introduction

For many years, 3 mol% yttria-stabilized zirconia (3Y-TZP) ceramic materials have emerged as biomedical materials. However, 3Y-TZP is a biologically inert ceramic material (Ke *et al.*, 2017). No biological links form between the implant component and nearby host tissues when 3Y-TZP is inserted into a human body (Kishi *et al.*, 2006). Due to the absence of biological linkage, problems occur in implant fixation and osseointegration after implantation (Viceconti *et al.*, 2000). So, such shortcomings can be addressed by making it bioactive from bio-inert. Generally, incorporating bioactive ingredients such as calcium phosphate (CaP), bioactive glass (BG), HA, and wollastonite is a significant alternative to impart bioactivity to 3Y-TZP ceramic and optimize osseointegration (Viceconti *et al.*, 2000) (Cortés-Hernández *et al.*, 2006) (Nogiwa-Valdez *et al.*, 2006). Many researchers make bioactive 3Y-TZP ceramic from bio-inert 3Y-TZP by incorporating bioactive glasses and report that 3Y-TZP-based BG composite is a bioceramic composite material (Ho *et al.*, 2011) (Habibe *et al.*, 2009) (De Paula *et al.*, 2019). Some researchers have also studied the effect of BG addition on the biological behavior of 3Y-TZP ceramics and found that BG addition into 3Y-TZP ceramics improves the cell proliferation of the bioceramic composites (Silver *et al.*, 2001) (Legeros *et al.*, 1993). Ions emitted by bioactive glasses enhance cell proliferation, osteoblast development, and angiogenesis. However, bioactive glass has a high bone formation rate and may make a new link in a matter of hours (Silver *et al.*, 2001). The antibacterial response of BG is related to many factors like changes in pH, dissolution rate, changes in concentration of alkali ions in glass composition, and bacterial species (Zhang *et al.*, 2010) (Allan *et al.*, 2001) (Zehnder *et al.*, 2006). The additional advantage of bioactive glass addition with 3Y-TZP ceramic materials is to reduce the final sintering temperature of the composite materials and leads to lowering the

implant manufacturing cost while retaining the biocompatibility (Ho *et al.*, 2011) (Habibe *et al.*, 2009) (De Paula *et al.*, 2019). Generally, bioactive glass is expected to occupy the interstices and voids of zirconia, which may reduce the interior porosity and enhance mechanical characteristics at lower sintering temperatures (Bicalho *et al.*, 2011). The bioactive glass 13-93 BG contains 53 SiO_2, 6 Na_2O, 12 K_2O, 5 MgO, 20 CaO, and 4 P_2O_5 (wt %) (Nawaz *et al.*, 2021). In comparison to other BGs, 13-93 BG has more SiO_2 and extra network modifiers, including K_2O and MgO. The extra network modifiers significantly impact the reaction kinetics of bioactive glass surfaces and new bone formation (Nawaz *et al.*, 2021). On the other hand, 13-93 bioactive glass has a lower thermal expansion coefficient, similar to TiO_2, and improves adherence to the substrates (Beltrán *et al.*, 2020). In this chapter, the effect of 13-93 BG additions on the structural, mechanical, *in-vitro* degradation, cell culture, and antibacterial response of 3Y-TZP–based bioceramic composite materials are evaluated. The variations of compositions and sample identification are given in Table 3.1.

4.2 Results and discussion

4.2.1 Particle size, XRD, SEM, and FTIR analysis of the prepared precursors

The DLS method is used to examine the particle size distribution by volume in the prepared powders. In DLS, typical spherical particle models with a scattering angle of 90° are utilized. An aqueous solution of 3Y-TZP powder is created by dispersing in the acetone and placed under a probe sonicator. The 3Y-TZP ceramic has average particle sizes of 652 ± 91 nm. The particle size distributions of 3Y-TZP, are shown in Fig. 4.1(a). In the 3Y-TZP XRD pattern, a major tetragonal phase of ZrO_2 is found, as shown in Fig. 4.1(b). The SEM image of prepared

3Y-TZP shows fine powder particles with less agglomeration, as shown in Fig. 4.1(c). The major characteristic bands are located at 595, 961, 1637, 2966, and 3399 cm−1, as shown in Fig. 4.1(d).

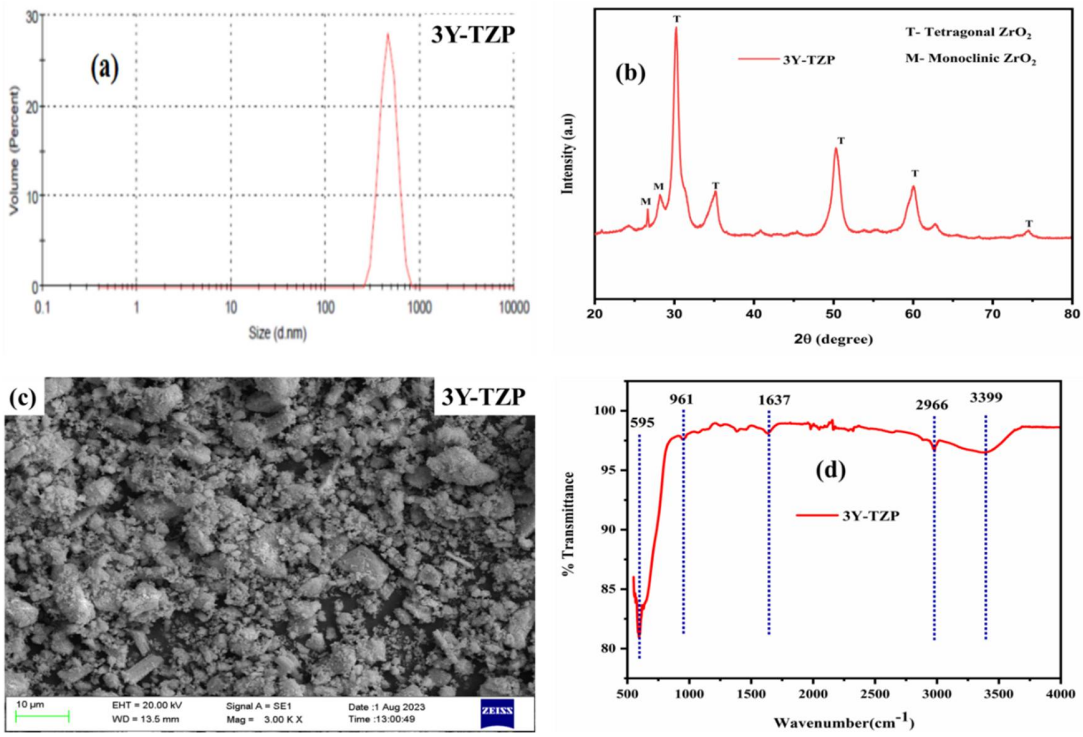

Fig. 4.1 (a-d) Characterization of prepared 3Y-TZP (a) Particle size distribution (b) XRD, (c) SEM images, and (d) FTIR.

The characteristic transmittance bands for Zr–O bonds appear at 595 cm−1 (Zehnder *et al.*, 2006). and 961 cm− 1 corresponds to Zr-O bonds (Bicalho *et al.*, 2011). These zirconium oxygen bonds indicate the existence of ZrO_2 in the synthesized samples. The characteristic bands located at 1637 cm−1 are caused by the adsorbed CO_2 from the air (Nawaz *et al.*, 2021) (Beltrán *et al.*, 2020). The characteristic band located at 2966 cm−1 is formed by the -C-H bonds (De Paula *et al.*, 2019). The entire process is performed in deionized water, as a result of which a strong Zr–OH transmittance band appears at 3399 cm−1 (Nawaz *et al.*, 2021) (Beltrán *et al.*, 2020).

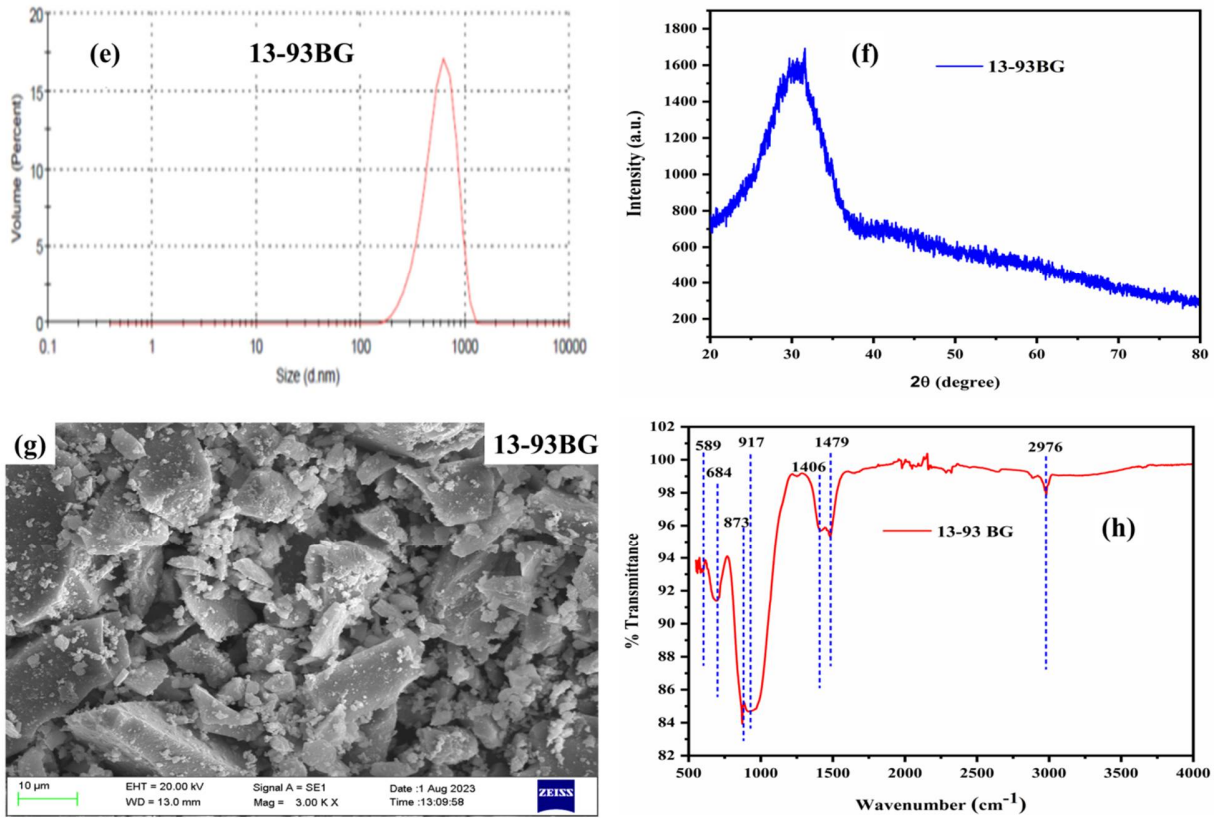

Fig. 4.1 (e-h) Characterization of prepared 13-93BG (e) Particle size distribution (f) XRD, (g) SEM images, and (h) FTIR.

Similarly, an aqueous solution of 13-93 BG powder is created by dispersing in the acetone and placed under a probe sonicator. The 13-93 BG have average particle sizes of 694 ± 194 nm. The particle size distributions of matrix and reinforce materials are shown in Fig. 4.1(e). In the 13-93 BG XRD pattern, no sharp peak is found, confirming that the bioactive glass powder is amorphous in nature, as shown in Fig. 4.1(f). In this pattern, a large hump between 22° to 38° is found and suggests a silica tetrahedron group. The SEM image of 13-93BG powder shows particles with a high agglomeration degree, as shown in Fig. 4.1(g). Fig. 4.1(h) shows the transmittance FTIR spectra of the calcined 13-93 BG powder at 589, 684, 873, 917, 1406, 1479, and 2976 cm^{-1}. Only the silica bands are visible in the result. The transmittance bands at wave

numbers 684, 873, and 917 cm^{-1} correspond to SiO_4 (Zehnder *et al.*, 2006) (Nowami *et al.*, 1999). Transmittance bands at 1406 and 1479 cm^{-1} correspond to the CO_3^{-2} group (Bicalho *et al.*, 2011) (Nawaz *et al.*, 2021) (Beltrán *et al.*, 2020) (Nowami *et al.*, 1999). The characteristic band located at 2976 cm^{-1} is caused by the -C-H bonds (De Paula *et al.*, 2019).

4.2.2 XRD and microstructural analysis of the sintered composites

Fig. 4.2(a) shows X-ray patterns of sintered 3Y-TZP/13-93 BG composites samples. The crystalline phases of ZrO_2 in the form of a monoclinic (m-ZrO_2) phase (reference code: 98-009-7971) and tetragonal (t-ZrO_2) phase (reference code: 98-003-0663) are present in this pattern. The volume percentage of t-ZrO_2 and m-ZrO_2 phases are calculated, as given in Table 4.1. Results indicate that the m-ZrO_2 phase is increased with the addition of BG contents, and it is found to be a maximum (76%) for the sample containing 25wt% of BG. Simultaneously, the t-ZrO_2 phase is decreased with increasing the BG contents and found to be a maximum (88%) for the pure 3Y-TZP sample. The formation of the m-ZrO_2 phase can be attributed to the undesirable martensitic transformation during the cooling of the sintered samples. This martensitic transformation promotes a volumetric expansion, which leads to micro-cracking and an increase in the formation of porosity in sintered samples during cooling (Ho *et al.*, 2011) (Habibe *et al.*, 2009) (De Paula *et al.*, 2019). Additionally, the X-ray pattern of the ZBG25 composite sample containing high BG content (25 wt%) indicates that there are some crystalline phases formed in the form of diopside (reference code: 98-011-1636), apatite (reference code: 98-001-2590) and dimagnesium phosphate hydroxide (reference code: 98-004-7403), as shown Fig. 4.2(b). Diopside ($CaMgSi_2O_6$) and apatite ($Ca_5(PO_4)_3(OH)$ are bioactive materials which are used in bone tissue engineering (Nowami *et al.*, 1999).

Table 4.1 Volume percentage of different phases (m-ZrO_2, t-ZrO_2), bulk densities, relative densities, and porosities of 3Y-TZP/13-93BG composites.

	ZBG0	ZBG5	ZBG10	ZBG15	ZBG25
m-ZrO_2 (Vol.%)	12	18	25	38	76
t-ZrO_2 (Vol.%)	88	82	75	62	24
Bulk density (gm/cc)	5.73±0.07	5.88±0.09	5.93±0.08	4.99±0.09	4.27±0.09
Relative density (%)	94.39±0.9	97.19±1.1	98.34±1.0	83.31±0.8	72.49±1.0
Porosity (%)	5.61	2.81	1.66	16.69	27.51

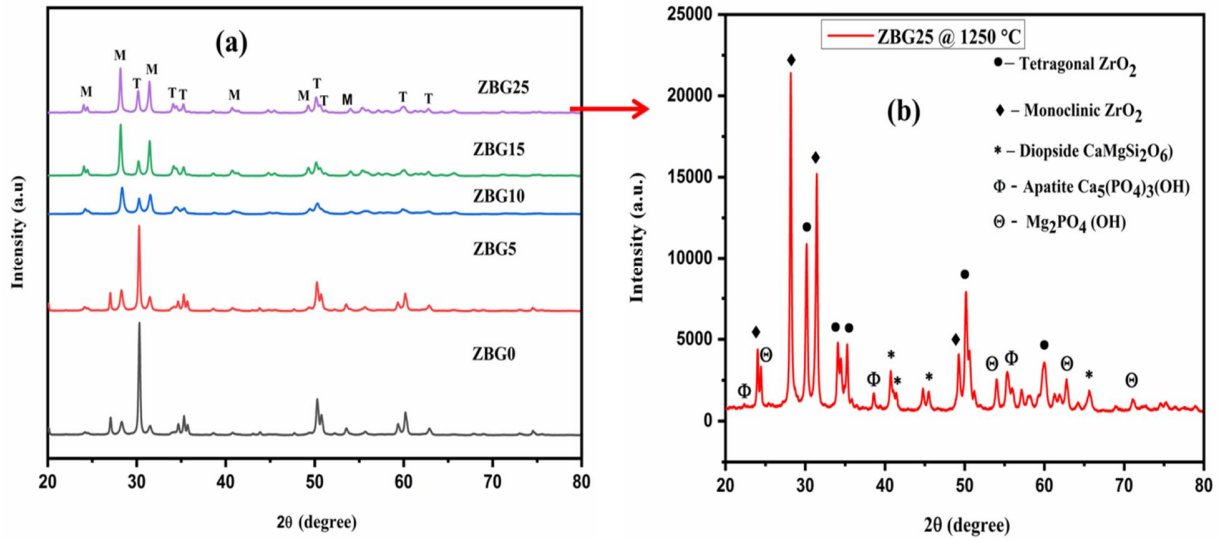

Fig. 4.2 XRD patterns of (a) sintered composite materials and (b) ZBG25 sample separately.

The SEM micrograph of 3Y-TZP-based biocomposite with the inclusion of 13-93BG (0 to 25 wt.%) is represented in Fig. 4.3(a)-(h). The loosened granules in Fig. 4.3(a) show that the pure

ZBG0 sample has not been sufficiently sintered at this temperature. Generally, pure high-density 3Y-TZP ceramic is sintered at 1450°C to 1550°C (Ho *et al.*, 2011) (Habibe *et al.*, 2009) (De Paula *et al.*, 2019). Improved sintering characteristics can be seen in the ZBG10 sample with 10 wt% BG inclusion, as shown in Fig. 4.3(c)-(d), suggesting that the BG frit effectively improves the sintering process at lower sintering temperatures. The SEM micrographs of ZBG5, ZBG10, ZBG15, and ZBG25, represented in Fig. 4.3(b)-(h), suggest that the BG frits are well-wetted the crystalline grain and also infiltrated into intergranular spaces. Due to the wetness of BG particles, the composite powders are compacted by agglomeration, as shown by the square mark in SEM images in Fig. 4.3(b)-(h). It is also observed that grain size is decreased with increasing the BG content into pure 3Y-TZP ceramic. The grain sizes (µm) of all samples are calculated using Image J software, and the values are 0.8, 0.8, 0.6, 0.4, and 0.5 µm, corresponding to samples ZBG0, ZBG5, ZBG10, ZBG15 and ZBG25, respectively.

Further, it is also observed that the grain shape is gradually changed from a polygon to a circular shape with increasing BG contents, indicating a change in the specimens' sintering behaviour; it may also be due to the eventually dissolved ZrO_2 grains (Ho *et al.*, 2011) (Habibe *et al.*, 2009). When glass frits are added, the flow becomes viscous at the sintering temperature. The porosities present in the samples are filled by the infiltration of viscous flow of BG frits, which consequentially may enhance the densification. According to the concept of liquid phase sintering (Ho *et al.*, 2011), viscous flow thoroughly wets the solid particles, creating a lot of capillary pressure in the narrow channels. It helps in densification by rearranging the particles to achieve better packing and by creating a quick diffusion path between the particles, where the mass transfer occurs via a dissolution-reprecipitation mechanism. The corresponding EDS mapping images of all samples are shown in Fig. 4.3(i)-(m). There are different elements present

in the composite samples, such as Zr, Y, Si, Ca, Na, Mg, K, P, and O, due to BG glass composition. It also offers that all the elements are dispersed evenly without extra impurity elements. Results represent that the wt% of the Zr element is decreased with increasing the BG concentration.

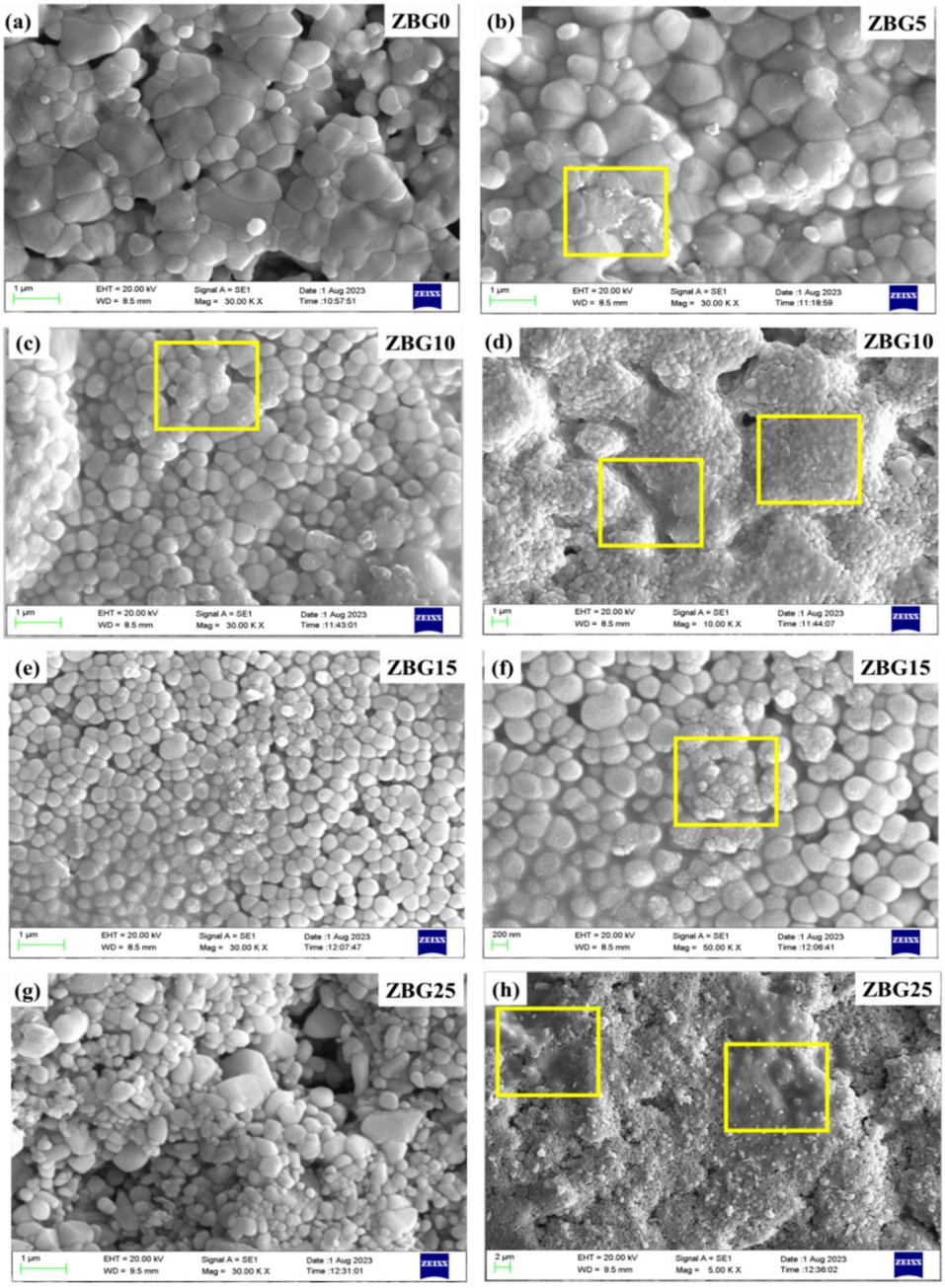

Fig. 4.3 (a)-(h) SEM images of 3Y-TZP-based biocomposite materials sintered at 1250℃.

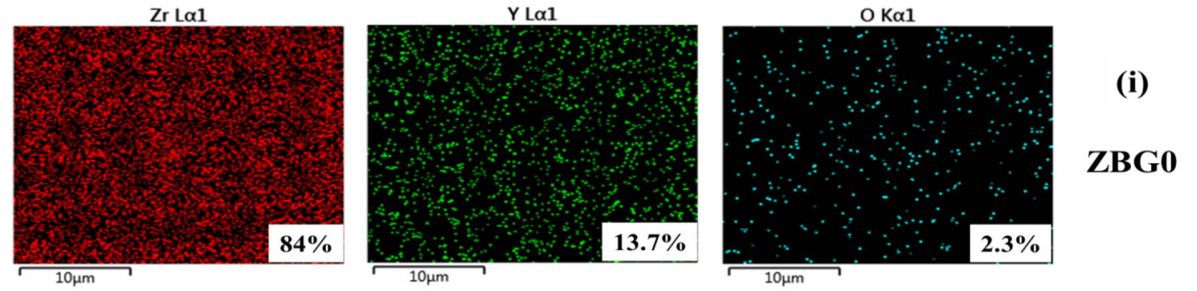
Zr Lα1
84%
10μm
Y Lα1
13.7%
10μm
O Kα1
2.3%
10μm
(i)
ZBG0

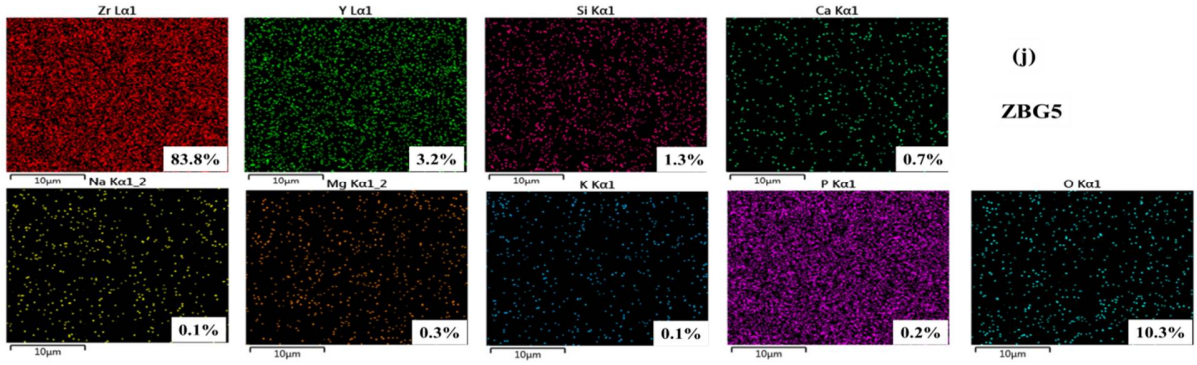
Zr Lα1
83.8%
Y Lα1
3.2%
Si Kα1
1.3%
Ca Kα1
0.7%
(j)
ZBG5
Na Kα1_2
0.1%
Mg Kα1_2
0.3%
K Kα1
0.1%
P Kα1
0.2%
O Kα1
10.3%

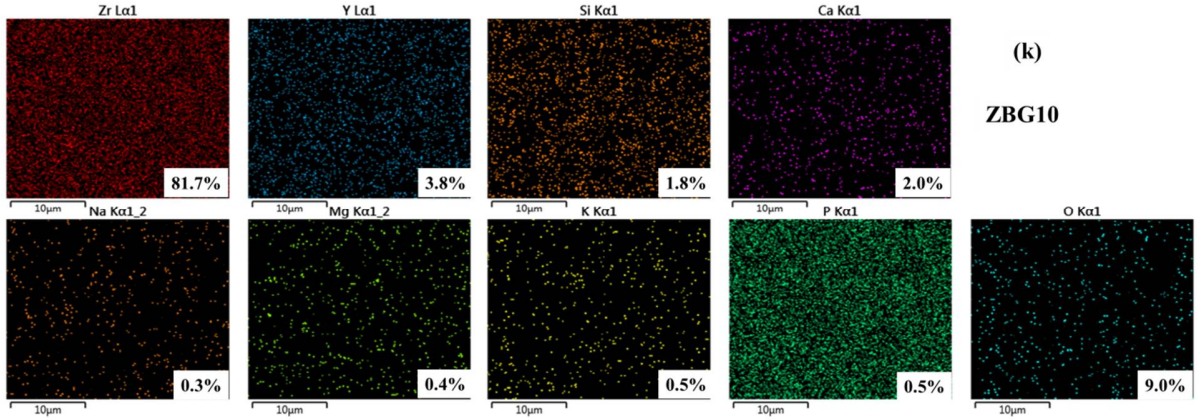
Zr Lα1
81.7%
Y Lα1
3.8%
Si Kα1
1.8%
Ca Kα1
2.0%
(k)
ZBG10
Na Kα1_2
0.3%
Mg Kα1_2
0.4%
K Kα1
0.5%
P Kα1
0.5%
O Kα1
9.0%

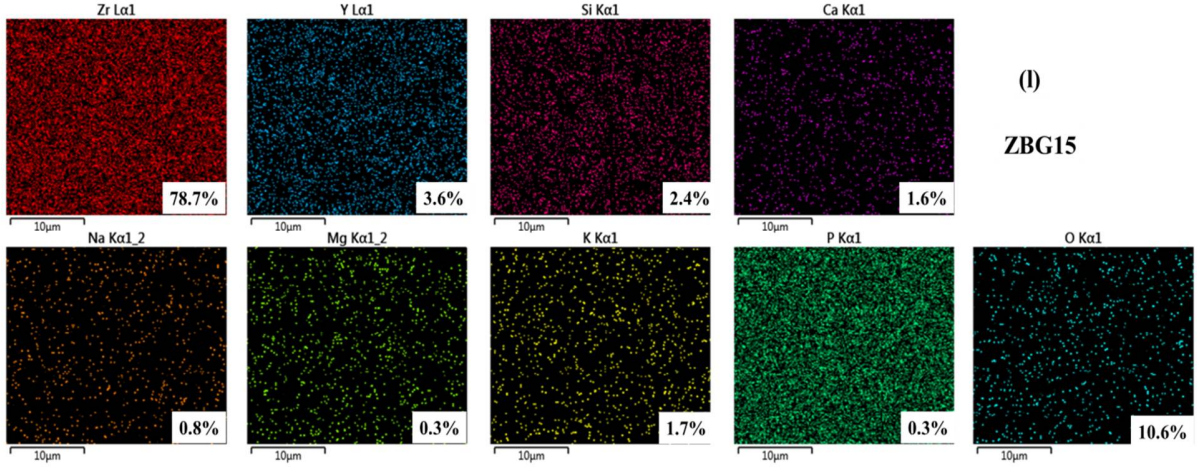
Zr Lα1
78.7%
Y Lα1
3.6%
Si Kα1
2.4%
Ca Kα1
1.6%
(l)
ZBG15
Na Kα1_2
0.8%
Mg Kα1_2
0.3%
K Kα1
1.7%
P Kα1
0.3%
O Kα1
10.6%

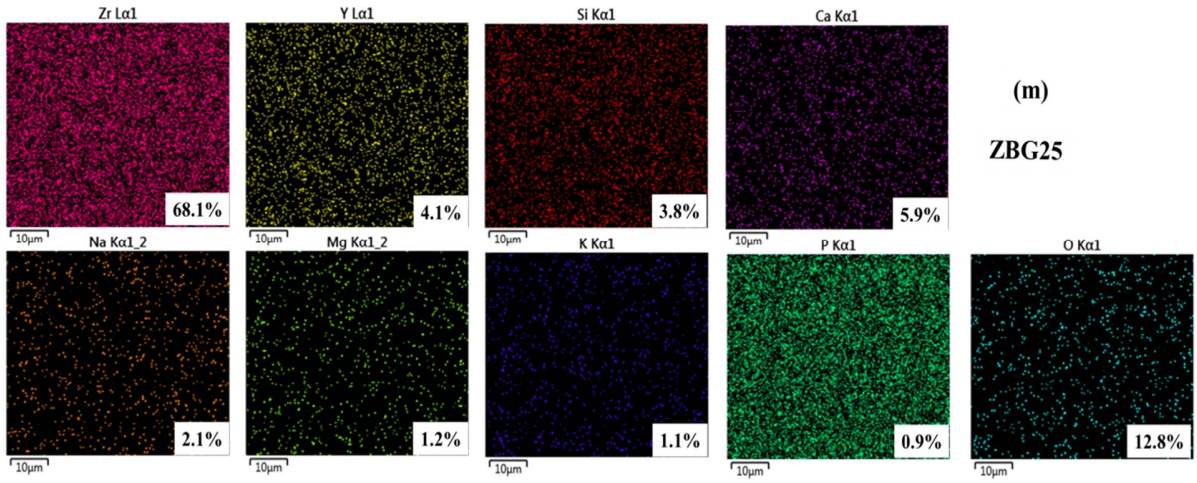

Fig. 4.3 (i)-(m) EDS mapping images of 3Y-TZP-based biocomposite materials sintered at 1250°C.

4.2.3 Density and mechanical properties of sintered composites

The bulk densities of 3Y-TZP and 3Y-TZP/13-93 BG composite materials are shown in Table 4.1, and the mechanical properties are shown in Table 4.2. The results show that bulk density increases with increasing the BG contents up to 10 wt%. With further BG addition, the bulk density is decreased up to 25 wt% of BG additions. Further, the relative densities of the sintered samples are calculated and found to have the same trend as bulk density. At 1250°C, the relative density of ZBG0, ZBG5, ZBG10, ZBG15, and ZBG25 samples are observed 94.39%, 97.19%, 98.34%, 83.31%, 72.49%, respectively. The maximum value of relative density is found in the ZBG10 sample, and the minimum in the ZBG25 sample. The percentage of porosity of the sintered samples is calculated and given in Table 4.1. The results indicate that with increasing BG content into 3Y-TZP, the porosity is decreased up to 10 wt% afterward; it increases up to 25% of BG addition. The flexural strength and compressive strength of 3Y-TZP and 3Y-TZP/13-93 BG composite materials initially increase with increasing the BG contents up to 10 wt%. With

the addition of BG amounts up to 10 wt%, the compressive strength of the composite attains the peak value of 488.7 MPa, which is enhanced by 26.39 % compared to pure 3Y-TZP ceramic. With further BG addition, the compressive and flexural strength is decreased up to 25 wt% of BG additions. The hardness is increased with BG addition in 3Y-TZP ceramics. It is well known that hardness is a surface property of materials. It is strongly affected by adding BG contents into 3Y-TZP ceramic (Habibe *et al.*, 2009). So, it is clearly observed that up to 10 wt% of BG additions, the relative density, and all the mechanical characteristics of 3Y-TZP/13-93 BG ceramic composite material are significantly improved.

Table 4.2 Mechanical properties of 3Y-TZP/13-93BG composites.

S. No.	Sample Code	Flexural strength (σ_f) MPa	Compressive strength (σ_c) MPa	Hardness (GPa)
1.	ZBG0	298.7 ± 29.3	386.7 ± 32.4	5.9 ± 0.5
2.	ZBG5	310.4 ± 35.1	409.1 ± 41.7	6.8 ± 0.5
3.	ZBG10	397. 9 ± 41.8	488.7 ± 33.7	8.5 ± 0.9
4.	ZBG15	367.4 ± 43.7	413.3 ± 47.1	8.9 ± 0.8
5.	ZBG25	309.2 ± 38.3	375.2 ± 40.1	9.0 ± 1.2

Many researchers have stated that adding BG into low-temperature sintered 3Y-TZP ceramics enhances the densification of composite (Ho *et al.*, 2011) (Habibe *et al.*, 2009) (De Paula *et al.*, 2019) (de Oliveira *et al.*, 2021). Consequently, mechanical properties are improved. It may result from better dispersion of semi-liquid glass due to lowering the viscosity that may enable the removal of pores and reduce the unwanted gathering of glassy phase in the composite

(Ho *et al.*, 2011) (Habibe *et al.*, 2009) (De Paula *et al.*, 2019). Generally, the sintering temperature of pure 3Y-TZP ceramic is 1450^{o}C to 1550^{o}C to achieve maximum densification, as reported by previous researchers (Ho *et al.*, 2011) (Habibe *et al.*, 2009) (De Paula *et al.*, 2019). In this work, the 3Y-TZP ceramic is sintered at 1250^{o}C. Some porosity may be present at the lower sintering temperature, leading to lower relative densities and low mechanical properties (Ho *et al.*, 2011) (Habibe *et al.*, 2009) (De Paula *et al.*, 2019) (de Oliveira *et al.*, 2021). When BG contents are added to 3Y-TZP ceramic up to 10 wt%, it may fill the porosity of 3Y-TZP ceramic. Table 4.1 indicates that porosity is reduced up to 10 wt% of BG addition and increases up to 25 wt% of BG. Due to this, densification is improved consequentially, and mechanical properties are also improved. The mechanical properties are strongly dependent on porosity (Luo *et al.*, 1999). The formation of the m-ZrO_2 phase increases with the addition of BG contents (Habibe *et al.*, 2009). At the microstructure level, it is also observed that the semi-liquid BG is wetted and infiltrated into the interspaces between the grains, as shown in Fig. 4.3(b, d, and f). The decrease in relative density and mechanical properties after x = 10 wt% is due to an increase in the creation of porosity in the matrix due to martensitic transformation and also due to more glassy phases present in the composite samples (Habibe *et al.*, 2009) (de Oliveira *et al.*, 2021). It may be due to the unwanted gathering of the glassy phase, which helps to create residual stress during cooling and results in crack propagation (Ho *et al.*, 2011) (Habibe *et al.*, 2009) (De Paula *et al.*, 2019) (de Oliveira *et al.*, 2021).

4.2.4 Biodegradation and bioactivity study

4.2.4.1 pH analysis

Fig. 4.4(a) represents the variation of pH value of 3Y-TZP/13-93BG bioceramic composites during soaking in the SBF solution for up to 35 days. For all the samples, the starting pH of SBF is kept at 7.40.

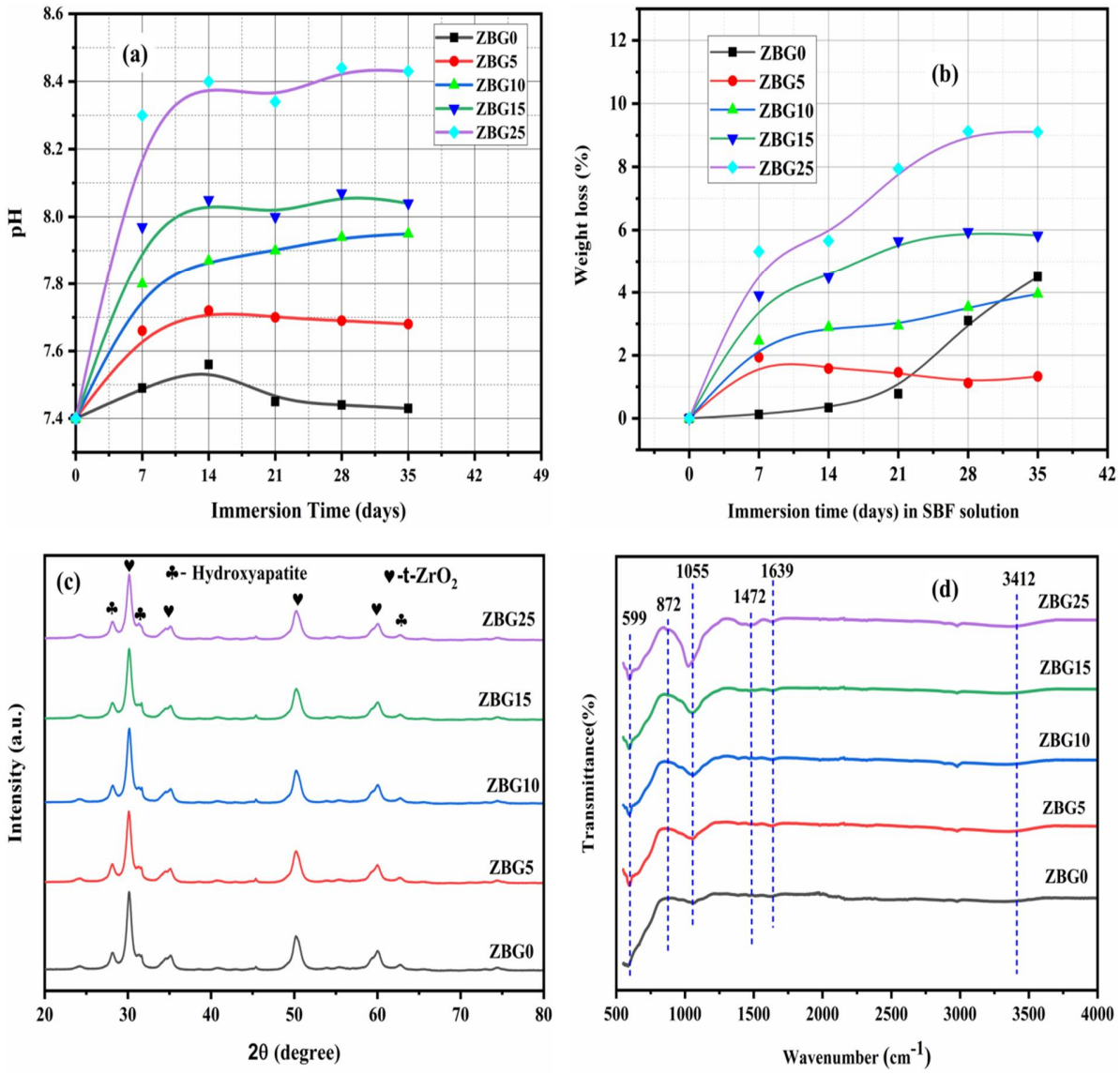

Fig. 4.4 (a) pH measurement for different time intervals, (b) In-vitro biodegradability analysis, (c) XRD result after 35 days of immersion in SBF, (d) FTIR spectra after 35 days of immersion in SBF.

The results indicate that for all the samples, the pH of the SBF solution first rises up to 14 days afterward; it follows a constant trend with increasing the immersion time in the SBF solution. Further, it is also observed that the pH of all composite samples is increased with increasing the BG concentration for all immersion days. The interaction of ions such as Na^+, Ca^+, K^+, etc., present in the samples along with cations of SBF (H^+ or H_3O^+) forms a negatively charged surface that attracts Ca^{2+} ions present in SBF, which may be the cause of the pH raising tendency for all composite samples (Mohammadi *et al.*, 2021). The amounts of released ions are increased with increasing the BG concentration in the pure 3Y-TZP sample, leading to an enhancement of the pH of the composite samples (Mohammadi *et al.*, 2011). The phosphate and calcium in the composite samples form an HA layer over the submerged sample. Once the apatite is formed, the pH variation follows an almost constant pattern as immersion time is increased (Fathi *et al.*, 2007) (Li *et al.*, 2005). The XRD [Fig. 4.4(c)], FTIR [Fig. 4.4(d)], and SEM with EDS [Fig. 4.5] of all samples support the HA layer's deposition on the immersed samples.

4.2.4.2 Biodegradation analysis

In-vitro degradation is an important criterion for synthetic biomedical materials because the appropriate concentration of Ca^{2+}, $P^{5+,}$ and Si^{4+} ions have essential functions in osteogenesis (Hoppe *et al.*, 2003). Silicate-based biomaterials generally deteriorate by dissolution in an SBF solution medium (Vyas *et al.*, 2015). In this study, the 13-93BG incorporation is chosen to regulate the degradation rate of 3Y-TZP bioceramics, as shown in Fig. 4.4(b). Results represent that % W_L is increased with increasing the immersion time up to 28 days in SBF; after that, it follows the almost constant trend. Whereas % W_L also increases with increasing the

incorporation of BG concentration. The rise in % W_L occurs due to an ionic interaction between the substance and the SBF solution (Zhang *et al.*, 2022). For the ZBG5 and ZBG10 samples, the % W_L is almost near to the base ZBG0 sample, whereas it is increased by a significant amount for ZBG15 and ZBG25 samples. It may be due to the bulk density enhancement of the ZBG5 and ZBG10 samples in comparison to base sample ZBG0 due to the addition of the bioglass. Whereas the bulk density of ZBG15 and ZBG25 is decreased with increasing the bioglass incorporation up to 25 wt% into base 3Y-TZP ceramics. Researchers have reported that some physical variables, like decreased densification and decreased particle size, encourage biodegradation (Devi *et al.*, 2017) (Sarkar *et al.*, 2019). The decreased densification enhances the porosity and the surface area, which promotes ionic interaction between the samples and the surrounding media, resulting in faster dissolution (Devi *et al.*, 2017) (Sarkar *et al.*, 2019).

4.2.4.3 Bioactivity analysis

After 35 days of soaking in SBF solution, the surface morphology with EDS spectra of all the samples is shown in Fig.4.5. There is no significant evidence of apatite mineralization on the surface of the ZBG0, as represented in Fig. 4.5(a). The considerable mineralization potential of the 3Y-TZP/13-93BG composite samples is amply demonstrated by the *in-vitro* bioactivity data, as shown in Fig. 4.5(b to e). After putting the samples in SBF, an additional layer is formed with the typical HA appearance. FE-SEM morphology of all the samples indicates that the apatite mineralization ability is increased with increasing the BG content into pure 3Y-TZP ceramic. The Ca, P, and O, which are essential parts of bone apatite, are observed in the EDS spectra of the all-composite samples. The development of an HA on the 3Y-TZP/13-93BG composite samples is also confirmed by XRD, as shown in Fig. 4.5(c). After 35 days of soaking, the XRD

of all samples shows the crystalline phase of HA (Reference Code: 98-006-0211) in this pattern. The HA formation is also confirmed by FTIR, as represented in Fig. 4.4(d). The FTIR spectra indicate the apatite layer formation in all 3Y-TZP-based composites. In FTIR spectra, transmittance peaks are located at 599, 872, 1055, 1472, 1639, and 3412 wavenumbers (cm^{-1}). Transmittance bands at 599 and 1055 cm^{-1} are attributed to phosphate bands (PO_4^{-3}) (Luo *et al.*, 1999) (Rameshbabu *et al.*, 2005). The presence of PO_4^{-3} ions over the composite samples confirms the apatite layer development. The presence of carbonate ions is indicated by the transmittance bands at 872 and 1472 cm^{-1}. The carbonate ion may be formed by a reaction between carbon dioxide and a high-pH solution (Rameshbabu *et al.*, 2005). At 1639 and 3412 cm^{-1}, the OH^- band is formed (Yadav *et al.*, 2020) (Rameshbabu *et al.*, 2005. Apatite formation and dissolution in SBF are confirmed by variations in band intensity (Rameshbabu *et al.*, 2005). It is reported that when the BG concentration is increased in the base ZBG0, the rate of ion interaction is increased (Hoppe *et al.*, 2011). As a result, the frequency of causing HA deposition over composite materials is increased. For ZBG0 and ZBG5, no significant HA peak is found, which is due to very thin HA layer formation. The process by which the apatite layer forms on the composite samples may be similar to the bioglass system. The surface-formed hydrated silica (Si-OH) serves as the primary site for apatite nucleation, followed by the dissolution. An ionic interaction occurs between the surface-bound Ca^{2+} ions and PO_4^{3-} ions present in SBF, which results in the development of the HA layer (Mohammadi *et al.*, 2021) (Zhang *et al.*, 2022). When the BG addition is increased, more BG particles penetrate into the 3Y-TZP. It enhances the release of Ca ions and increases the rate of HA formation (Mohammadi *et al.*, 2021) (Zhang *et al.*, 2022).

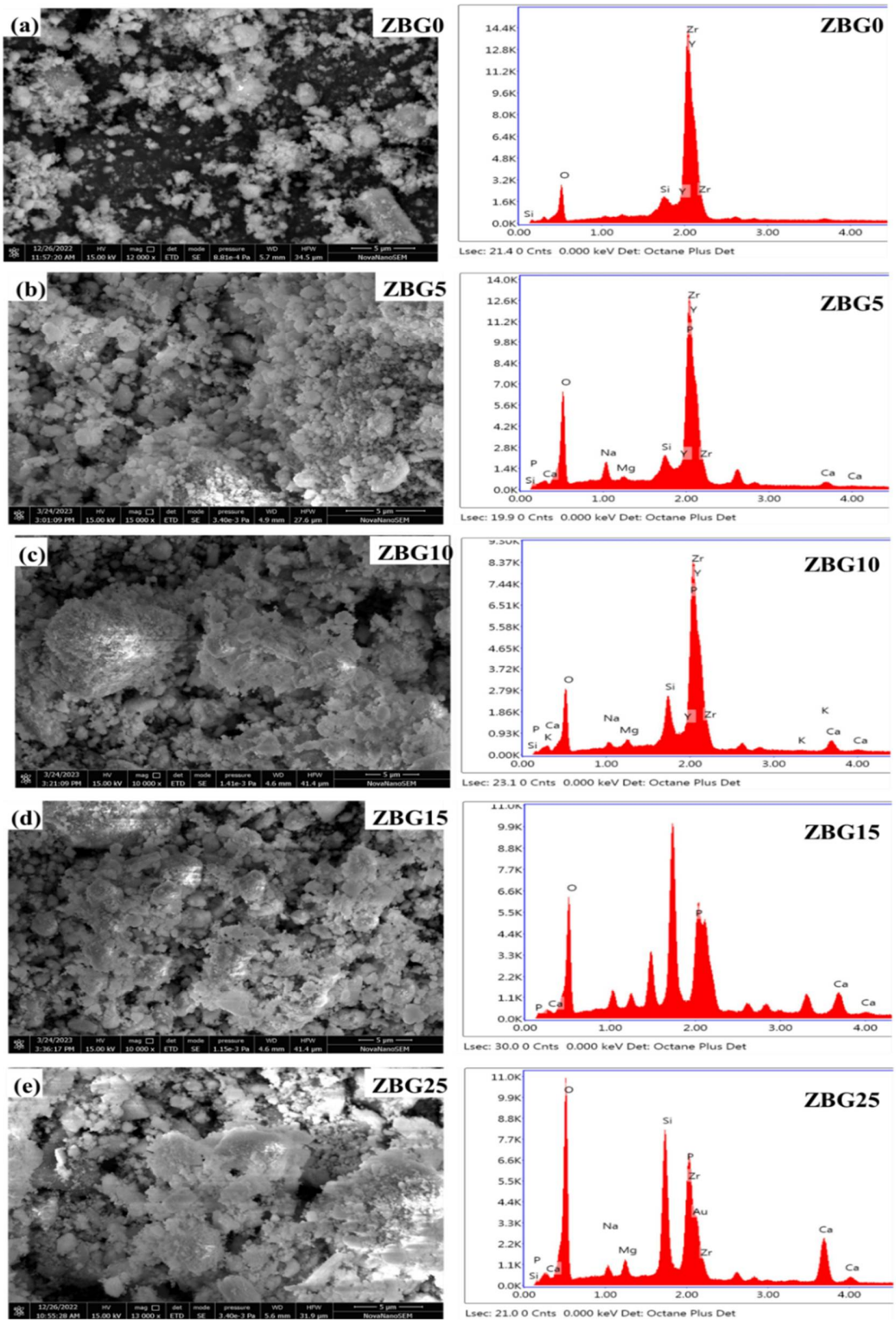

Fig. 4.5 FE-SEM images with EDS spectra of different samples after 35 days of immersion in SBF.

4.2.4.4 Cell culture study

4.2.4.4.1 MTT assay

The viability of MG-63 cells, cultured for 3, 5, and 7 days on the surfaces of [(100-x) (3Y-TZP) – x (13-93 BG)] (where x = 0 to 25 wt. %), samples and control were quantitatively assessed in the form of cell proliferation, as shown in Fig. 4.6. The cell viability is observed to increase with increasing the incubation period for all tested samples, representing good cytocompatibility. Further, it is also observed that higher viability is found on the surfaces of composite samples in comparison to the pure 3Y-TZP samples for all 3, 5, and 7 days of incubation periods. Among all samples of 3Y-TZP, the viability of MG-63 cells on the surfaces of [(100-x) (3Y-TZP) – x (13-93 BG)] (where x = 0 to 25 wt. %), samples is calculated to be 134, 144, 150, and 150%, after 3 days of incubation. However, after 5 and 7 days of incubation, the viability of all samples is increased by 119, 125, 137, and 141% and 115, 120, 129, and 132 %, respectively, in comparison to pure base sample ZBG0, respectively. After being incubated for 3, 5, and 7 days, the optical densities of all the composite samples, apart from the pure ZBG0 base sample, display a noticeable improvement as compared to the control sample [correspond to (*) in Fig. 4.6)]. After 3, 5, and 7 days of incubation, the optical densities of all bio composite samples have shown considerable improvement as compared to the base ZBG0 sample [correspond to (#) in Fig. (4.6)]. Additionally, after incubation for 3, 5, and 7 days, the optical densities of the composite ZBG10, ZBG15, and ZBG25 samples show a noticeable improvement in comparison to the base ZBG5 sample [correspond to (**) in Fig. (4.6)]. The result indicates that the inclusion of BG into base ZBG0 sample enhances the proliferation of MG-63 cells, which is also supported by the fluorescence microscopy images, as shown in Fig. 4.7. In *in-vitro* cell culture, 3Y-TZP/13-93 BG composite samples release Ca^{2+}, PO_4^{-3} and Si^{4+} ions into the

culture media, which form a Si-rich layer on the base samples (Verma *et al.*, 2020). Meanwhile, a significant negative charge is produced, which is capable of absorbing proteins in the culture media and, therefore, stimulating cell proliferation. Overall, it is evident that the cellular response of 3Y-TZP-based bioceramic composite can be significantly improved by the BG addition into pure 3Y-TZP ceramic.

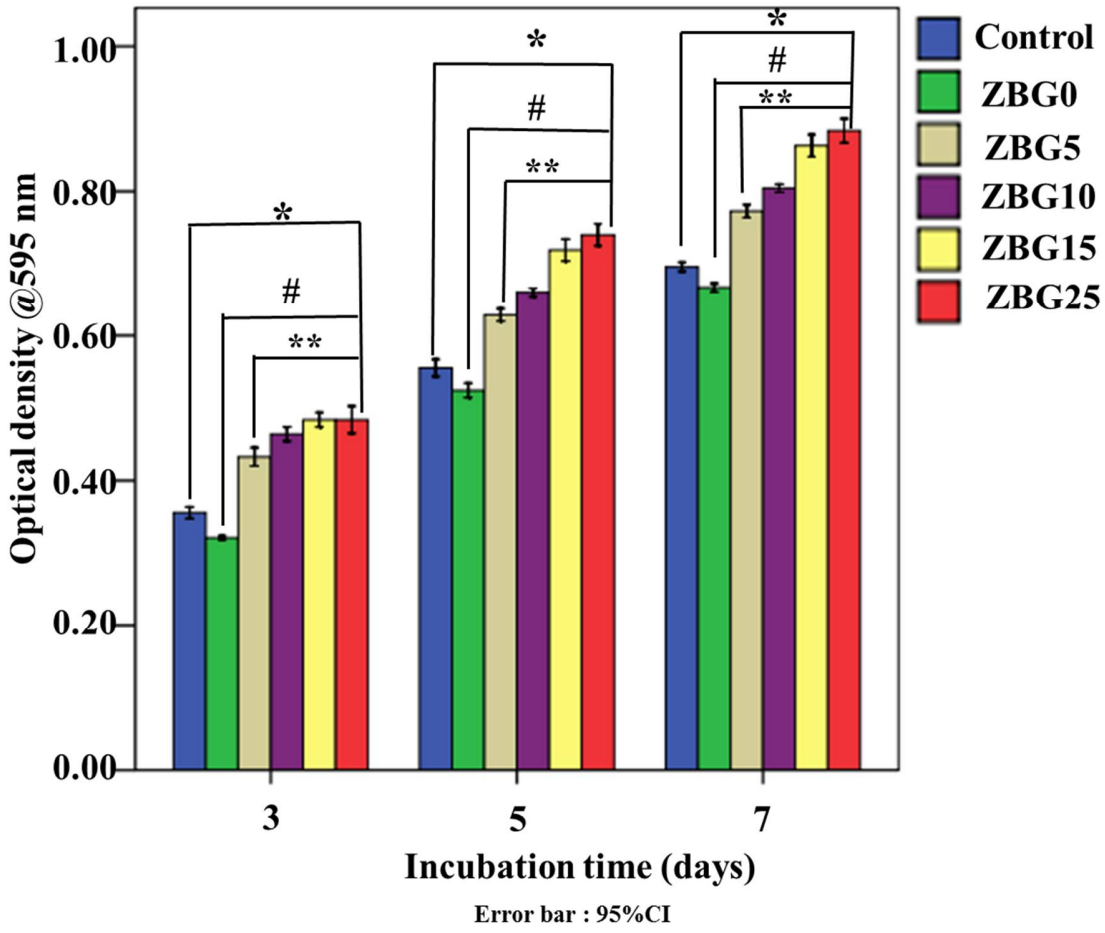

Fig. 4.6 MTT assay result for 3Y-TZP/13-93 BG bioceramic composite, cultured for 3, 5 and 7 days. The symbol '*****' represents the statistically significant difference in the mean optical density for all samples in comparison to the control sample, and '#' represents the statistically significant difference in the mean optical density for all bio-composite

samples in comparison to the base samples ZBG0. **'**'** represents the statistically significant difference in the mean optical density for ZBG10, ZBG15, and ZBG25 samples in comparison to ZBG5 sample.

4.2.4.4.2 Fluorescence microscopy study

The response of the MG-63 cells on the samples of pure 3Y-TZP, 3Y-TZP/13-93 BG composites, and control sample were qualitatively examined via morphological analyses of adhered cells, as depicted in Fig.4.7. It is observed that cell density is higher on the surface of 3Y-TZP/13-93 BG composites as compared to pure 3Y-TZP ceramic. In addition, the densities of cells on 3Y-TZP/13-93 BG surfaces increase with an increase in BG concentration (0 to 25 wt% of BG) in pure 3Y-TZP ceramics. The cells appear to be less dense and flattened on the ZBG0 sample in comparison to the control sample. Further, the cells appear to be more dense in increasing order of ZBG5, ZBG10, ZBG15, and ZBG25 in comparison to pure ZBG0 samples. The highest cell density is found for the ZBG25 sample. It has been reported that pure 3Y-TZP ceramics are bio-inert and do not promote cellular functionality (Zhang *et al.*, 2022). It has also been reported that BG addition into 3Y-TZP ceramics improves the cell proliferation of the bioceramic composites (Silver *et al.*, 2001) (Legeros *et al.*, 1993). Ions released by bioactive glasses enhance cell proliferation, osteoblast development, and angiogenesis. Osteoblasts are the functional and structural components of bone development and metabolism (Valerio *et al.*, 2004). Due to ionic exchange, the release of silicilic acid by silicate-based bioglass results in the alkaline nature of the culture media (Xynos *et al.*, 2000) (Silver *et al.*, 2001) (Bosetti *et al.*, 2003). Despite the belief that such an event would be harmful to cells, an increase in osteoblast viability and proliferation is observed. This is consistent with earlier reports, which demonstrated

an association between alkalinization and the growth of osteoblasts or chondroblasts (Vrouwenvelder *et al.*, 1992). Additionally, it is shown that the cell membrane contains voltage-activated calcium channels (Valerio *et al.*, 2004) and that channel sensitivity is increased by alkalinization, facilitating cellular calcium entrance (Rhee *et al.*, 2003) (Seaborn *et al.*, 2002). This is consistent with our observation of accelerated proliferation in the presence of ionic compounds, which are released from silicate-based bioglass in the medium.

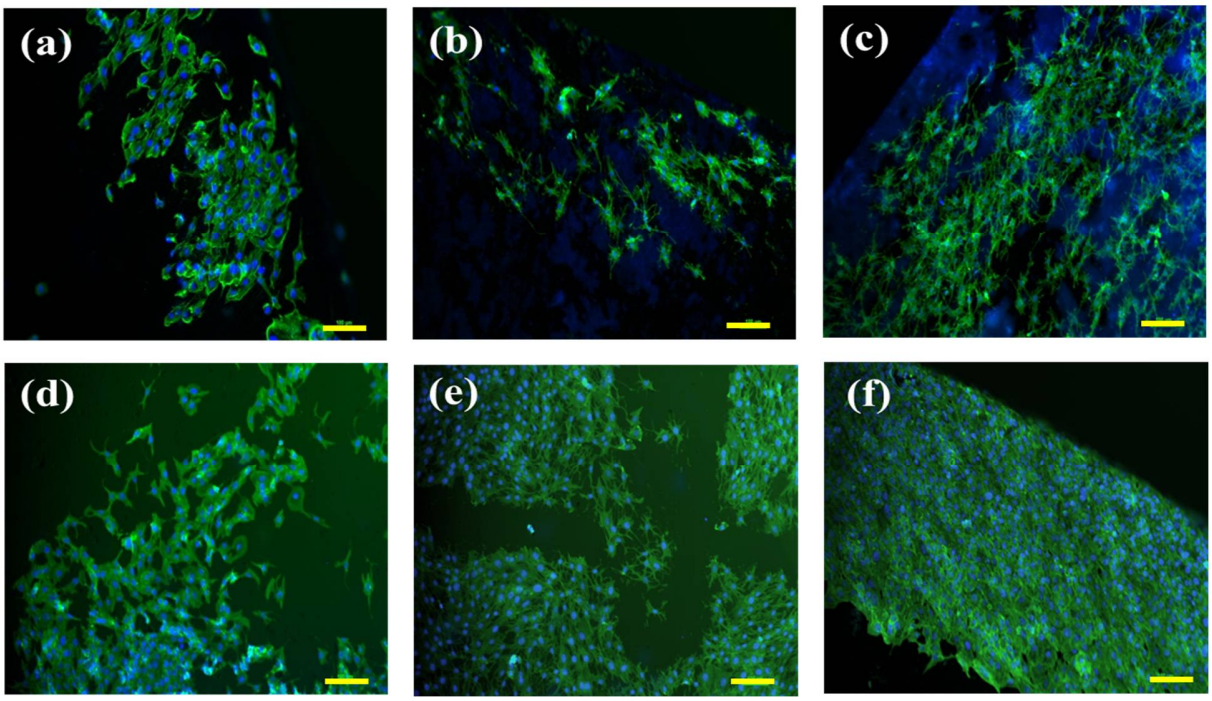

Fig. 4.7 Florescence microscopy images of MG-63 cells, adhered on 3Y-TZP/13-93 BG bioceramic composites, while cultured for 48 hours, (a) Control, (b) ZBG0, (c) ZBG5, (d) ZBG10, (e) ZBG15, (f) ZBG25. The scale bar represents 100 µm.

4.2.4.5 Antibacterial response

Fig. 4.8 illustrates the change in mean optical density (O.D.) of 3Y-TZP and 3Y-TZP -xBG (x = 0, 5, 10, 15, and 25 wt%) composite systems when it is exposed to E. coli and S. aureus bacteria. The mean O.D. of both E. coli and S. aureus bacteria cells decreases with the incorporation of BAG. Asterisks (*) and (#) represent the significant difference among all the samples with respect to control for E. coli and S. aureus bacteria, respectively, Fig. 4.8. Asterisks (@) and (&) represent the significant difference among the composite samples (ZBG5, ZBG10, ZBG15, and ZBG25) with respect to ZBG0 sample for E. coli and S. aureus bacteria respectively at $p \leq 0.05$, as shown in Fig. 4.8. 3Y-TZP –xBG composites decrease the mean O.D. significantly for S. aureus bacteria as compared to 3Y-TZP [Fig. 4.8]. On the surfaces of ZBG25, the density of S. aureus bacterial cells is decreased by about 30%. The live/dead ratio of 3Y-TZP and 3Y-TZP –xBG (x = 0, 5, 10, 15, and 25 wt%) composite systems is calculated against E. coli and S. aureus bacteria with the help of O.D. of samples. It is found that the live/dead ratio for E. coli and S. aureus bacterial cells decreases significantly with the addition of BG into 3Y-TZP. The live/dead ratio for E. aureus of ZBG0, ZBG5, ZBG10, ZBG15, and ZBG25 are 13.83, 4.93, 3.31, 2.28, and 1.80, respectively. The live/dead ratio for S. aureus of ZBG0, ZBG5, ZBG10, ZBG15, and ZBG25 are 15.33, 5.53, 3.63, 2.61, and 2.12, respectively. It can be observed from the antibacterial results analysis that BAG (x = 0, 5, 10, 15, and 25 wt%) addition to 3Y-TZP enhances the antibacterial properties of 3Y-TZP. The antibacterial effectiveness of BG is influenced by several factors, including alterations in pH, dissolution rate, variations in alkali ion concentrations within the glass composition, and the type of bacterial species involved (Zhang *et al.*, 2010) (Allan *et al.*, 2001) (Zehnder *et al.*, 2006). Notably, the antibacterial properties are notably impacted by elevations in solution pH (Zhang *et al.*, 2010) (Allan *et al.*, 2001) (Zehnder

et al., 2006). As the glass demonstrates an increased tendency to dissolve, local pH levels rise, along with alkali ion concentrations in the solution.

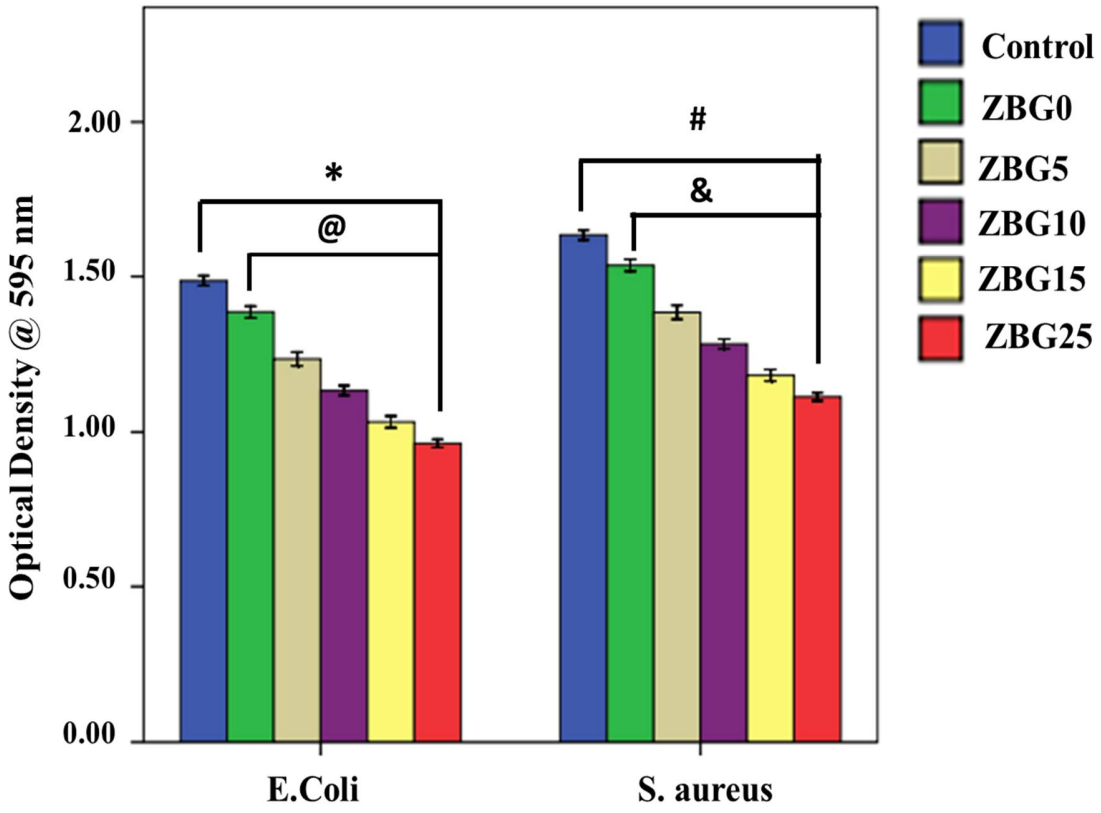

Fig. 4.8 Antibacterial response of 3Y-TZP and 3Y-TZP –xBG (x = 0, 5, 10, 15, and 25 wt%) composite for gram-negative (E. coli) and gram-positive (S. aureus) bacteria. Asterisks (*) and (#) represent the statistically significant difference among all the samples with respect to control for gram-negative (E. coli) and gram-positive (S. aureus) bacteria, respectively, at $p \leq 0.05$. Asterisks (@) and (&) represent the statistically significant difference among the composite samples (ZBG5, ZBG10, ZBG15, and ZBG25) with respect to the ZBG sample (ZBG0) for gram-negative (E. coli) and gram-positive (S. aureus) bacteria, respectively at $p \leq 0.05$.

These changes contribute to an overall enhancement of the glass's antibacterial capabilities (Zhang *et al.*, 2010) (Allan *et al.*, 2001) (Zehnder *et al.*, 2006). The findings from the *in-vitro* biomineralization study indicate that the pH and degradation rate of composite samples containing BG increase with higher concentrations of BG. This elevation in pH and degradation rate could potentially augment the antibacterial properties of 3Y-TZP -xBG composites. Furthermore, the presence of MgO in the BG composition contributes to the enhancement of antibacterial response (Stoor *et al.*, 1998) (Taeh *et al.*, 2022). Previous reports have suggested that the addition of MgO improves the antibacterial properties of 3Y-TZP, further supporting this observation (Stoor *et al.*, 1998) (Taeh *et al.*, 2022).

4.3 Summary

In the present investigation, the [(100-x) (3Y-TZP) – x (13-93 BG)] bioceramic composite materials are synthesized and analyzed for the structural, mechanical, *in-vitro* degradation, cell culture, and antibacterial behavior. The mechanical properties like flexural and compressive strengths of 3Y-TZP bioceramic composites have improved by 33.22% and 26.39%, respectively, compared to pure 3Y-TZP material. The hardness is enhanced with increasing bioactive glass addition. *In-vitro* biodegradability and bioactivity of modified 3Y-TZP-based bio-composite have been improved with increasing the inclusion of BG concentration. The cell proliferation and antibacterial response of modified 3Y-TZP-based bio-composite are enhanced with increasing the incorporation of BG concentration.